Reviewed Preprint
v1 • July 29, 2026
Not revised

For correspondence:
fanfan.zhou@sydney.edu.au
jian.li@monash.edu

Author notes: See page 21

Funding: See page 20

Reviewing editor: Warren Andrew Andayi, Murang'a University of Technology, Kenya

The structure-interaction model of polymyxin lipopeptides with human oligopeptide transporter 2

Xukai Jiang[1], Yining Luo[2], Mohammad AK Azad[3], Limei Xu[1], Min Xiao[1], Tony Velkov[3], Kade D Roberts[3], Visanu Thamlikitkul[4], Qi Tony Zhou[5], Fanfan Zhou[2] ✉, Jian Li[3] ✉

[1]National Glycoengineering Research Center, Shandong University, Qingdao, China • [2]Molecular Drug Development Group, Sydney Pharmacy School, Faculty of Medicine and Health, The University of Sydney, Sydney, Australia • [3]Biomedicine Discovery Institute, Infection Program, Monash University, Melbourne, Australia • [4]Division of Infectious Diseases and Tropical Medicine, Department of Medicine, Faculty of Medicine Siriraj Hospital, Mahidol University, Bangkok, Thailand • [5]Department of Industrial and Molecular Pharmaceutics, College of Pharmacy, Purdue University, West Lafayette, United States

eLife Assessment

This study presents a potentially **important** structure-interaction model describing recognition of polymyxin antibiotics by the human transporter hPepT2 and applies these insights to guide the rational design of potent polymyxin B analogues with reduced nephrotoxicity. The conclusions are supported by **compelling** evidence, integrating molecular dynamics simulations, transporter mutagenesis, uptake assays, protein expression analyses, antibacterial testing, and mouse nephrotoxicity studies, although some mechanistic interpretations remain limited by altered transporter expression and the absence of direct structural validation.

https://doi.org/10.7554/eLife.111387.1.sa3

Abstract

Background Multidrug-resistant (MDR) Gram-negative bacteria have triggered a critical global health crisis. Polymyxin lipopeptide antibiotics are used as a last-line therapy against these problematic pathogens, but their clinical use is largely limited by severe nephrotoxicity. Human oligopeptide transporter 2 (hPepT2) is a membrane transporter mediating the reabsorption of polymyxins in renal proximal tubular cells, substantially contributing to their nephrotoxicity. However, it remains unclear how polymyxins interact with hPepT2.

Methods In this study, we investigated the structure-interaction relationship (SIR) of polymyxins with hPepT2 by integrating computational, chemical and cell biology approaches. Bioinformatic modelling predicted the residues essential for the binding of polymyxins with hPepT2. Transporter mutagenesis and molecular analysis were employed to explore the role of each residue in the interaction of hPepT2 and polymyxins. Moreover, we synthesised a series of polymyxin-like analogues with altering the moieties that are critical for binding with hPepT2. The antibacterial activity and nephrotoxicity of these analogues were subsequently assessed.

Results Our bioinformatic modelling proposed an outward-facing structure of hPepT2 with a possible transport pathway that polymyxins bind to the lateral opening site of hPepT2 (e.g. E214, D215, D317, D342, E622). Molecular assays for transporter function and expression confirmed that D215 residue of hPepT2 is critical for polymyxin binding, while several other residues significantly impact on transporter turnover rate and/or protein expression. Our experimental validations showed that the lipopeptide analogues with altering the Dab1, Dab3, Dab5 and Dab9 moieties of polymyxins demonstrated decreased interactions with hPepT2. Among these synthetic analogues,

alanine substitution at Dab3 showed reduced nephrotoxicity in mice while reserved antibacterial activity against a range of bacterial strains.

Conclusions Overall, this proof-of-concept study demonstrated that the computationally predicted and experimentally validated polymyxin-hPepT2 SIR model provides a viable approach for the discovery of novel, safer lipopeptide antibiotics.

Introduction

The World Health Organization has highlighted antimicrobial resistance as an urgent threat to global public health (1). In particular, the Gram-negative 'superbugs' *Acinetobacter baumannii, Pseudomonas aeruginosa*, and *Klebsiella pneumoniae* can develop resistance to nearly all available antibiotics, posing some of the most serious challenges in modern medicine (2). Due to the lack of effective alternative antibiotics, polymyxins are often used as a last-line therapy against these 'superbugs' (3). However, polymyxins can cause nephrotoxicity in up to 60% of patients after intravenous administration, which is the major dose-limiting factor for their clinical use (4, 5). Thus, there is an urgent need for safer new-generation polymyxin lipopeptide antibiotics (6).

It has been demonstrated that polymyxin-induced nephrotoxicity is associated with extensive reabsorption into renal proximal tubular cells (4). The intracellular concentration of polymyxins in renal proximal tubular cells can be 5,000-fold higher than their extracellular concentration, which consequently leads to oxidative stress, autophagy, cell cycle arrest, and apoptosis (4). Therefore, the extensive reabsorption of polymyxins in renal proximal tubular cells is the very first step of nephrotoxicity.

Human Solute Carrier transporters (SLCs) are the primary influx transporters responsible for the cellular uptake of many drugs, including antibiotics (7, 8). There are over 300 SLC isomembers, among which SLCO, SLC22A and SLC15A are the key subfamilies mediating drugs moving across cell membrane (9, 10). Our previous study revealed that the cellular uptake of polymyxins is mediated through hPepT2 in the kidney (11), which is encoded by a key isoform of SLC15A subfamily, human oligopeptide transporter 2 *(hPepT2)* (10). This transporter protein is highly expressed in renal tubular cells mediating the uptake of polymyxins, with a comparable kinetic constant (K_m, reflecting transporter-substrate binding affinity) to its prototype substrates (10–12). It is one of the proton-driven symporters using the inwardly direct proton electrochemical gradient to drive the concentrative uptake of substrates across cell membrane (13). Substrates of hPepT2 include a range of di- or tri-peptides and peptide-like drugs, such as angiotensin-converting enzyme inhibitors (14). However, it remains unclear how hPepT2 recognise lipopeptide antibiotics, particularly polymyxins, which is critical for understanding its interaction with polymyxins contributing to their nephrotoxicity.

Here, we integrated computational and experimental approaches to elucidate the interaction relationship between hPepT2 and polymyxins. Importantly, we conducted a proof-of-concept chemical biological study by designing novel lipopeptides and evaluated their cellular uptake, nephrotoxicity, and antibacterial activities. This study establishes the first structure-interaction relationship (SIR) model for polymyxins and hPepT2, laying the foundation for rational drug design and discovery of novel lipopeptide antibiotics.

Results

MD prediction of the structural model of outward-facing hPepT2

We developed the three-dimensional structure of hPepT2 using AlphaFold2, as the outward structural model of hPepT2 (Fig. 1a) has not been experimentally solved. The putative overall structure adopted an inward open conformation (Fig. 1b), which disabled the exploration of the initial capture of polymyxins from the extracellular side of the membrane. Parker *et al.* demonstrated the Cryo-electron microscopy (Cryo-EM) structure of rat PepT2 with an outward open conformation (15). As rat PepT2 shares 83% sequence similarity with hPepT2, it is desired to be the prototype in the exploration of hPepT2 structure through the homologous modelling

algorithm. Upon remodelling, the resultant structure of hPepT2 adopted an outward open conformation (Fig. 1c). Several transmembrane domains (TMs) are involved in the formation of the solvent-accessible cavity for polymyxin translocation, including TM1, TM2, TM5, TM7, TM8 and TM10. The gate residue pairs (L75-R329, P341-E79, D170-S635 and K642-A177) marking the conformations were clearly indicated in the solvent-accessible regions on both the extracellular and intracellular surfaces (Fig. 1d). During 500-ns all-atom MD simulations with the inward-facing conformation as an initial configuration, the distances of the extracellular gate residue pairs L75-R329 and P341-E79 increased from 20 Å to 31 Å, and from 15 Å to 21 Å, respectively. Meanwhile, the distances of the intracellular gate residue pairs D170-S635 and K642-A177 decreased from 15 Å to 13 Å, and from 13 Å to 10 Å, respectively (Fig. 1e). Noteworthy, the conformational transition from the inward pose to the outward pose uncovered by MD simulations is consistent with the homologous model of rat PepT2 regarding the distance of extracellular and intracellular gate (15). This observation indicates the accuracy of the proposed model of hPepT2.

Polymyxin B binds to the lateral opening site of hPepT2 to enter the transport pathway

To further explore how hPepT2 recognises polymyxin molecules, we examined their interaction through long-time scale coarse-grained MD simulations. Although ten polymyxin B molecules were introduced to the simulation system, only one polymyxin molecule was observed to bind to the entrance of hPepT2 binding pocket, while the other polymyxin molecules attached to the membrane lipids (Fig. S3). Importantly, we discovered that there is a distinct pathway that polymyxins reached the extracellular lateral opening gate of hPepT2, as revealed by the simulation replicates (Fig. 2a and S4) with distinct equilibrated binding conformations (Fig. 2b). Our MD simulations predicted a possible transport pathway for polymyxins via hPepT2. Initially, polymyxin B attached to the plateau of TM1-TM6 helix bundle, mainly driven by the electrostatic interactions between the Dab5, Dab8 and Dab9 residues of polymyxin B and the E79, D208, E214 and D215 residues of hPepT2 (Fig. 3). Subsequently, polymyxin B translocated to the junction between the TM7-TM12 helix bundles and extracellular domains (ECDs) of hPepT2, where the Dab1, Dab3 and Dab5 residues of polymyxin B electrostatically interacted with the D342 and E555 residues of hPepT2. Polymyxin B then stabilised at the lateral opening gate of hPepT2 (i.e. lateral entry site), where the Dab8 and Dab9 moieties of polymyxin B electrostatically interacted with the D342 and E555 residues of hPepT2. Moreover, the hydrophobic atoms in Dab8 and Dab9 interacted with the F200, I201 and M204 residues of hPepT2, while the fatty acyl group of polymyxin B bound with the hydrocarbon tails of the phospholipid bilayer of the membrane.

To examine the detailed interactions between hPepT2 and polymyxin B, we performed all-atom MD simulations of the hPepT2-polymyxin B complex. During system preparation, the polymyxin B molecule was placed in four different poses within the complex to enhance sampling of binding dynamics. The results revealed that Dab1, Dab8, and Dab9 form strong electrostatic interactions with hPepT2, with interaction energies ranging from – 180 to –260 kJ/mol (Fig. 4), while Dab3 and Dab5 may also contribute significantly. Together with observations from the coarse-grained simulations, these results indicate that the positively charged Dab residues are key determinants of binding affinity to hPepT2.

Functional mutagenesis elaborates on the predicted transport pathway

At physiological pH, there are five positively charged residues (i.e. Dab residues) on the polymyxin molecule and we assumed that the key negatively charged residues of hPepT2 identified by the MD simulations (i.e. E79, D208, E214, D215, D317, D342, E555 and E622) may play crucial roles in the recognition and interactions with polymyxins. We employed functional mutagenesis to confirm their roles in the uptake of polymyxins, as predicted by our MD studies. Through the commonly used alanine-scanning mutagenesis approach, we constructed the correspondent mutants of hPepT2. Noteworthy, alanine substitution not only impacted on the side chain length of the

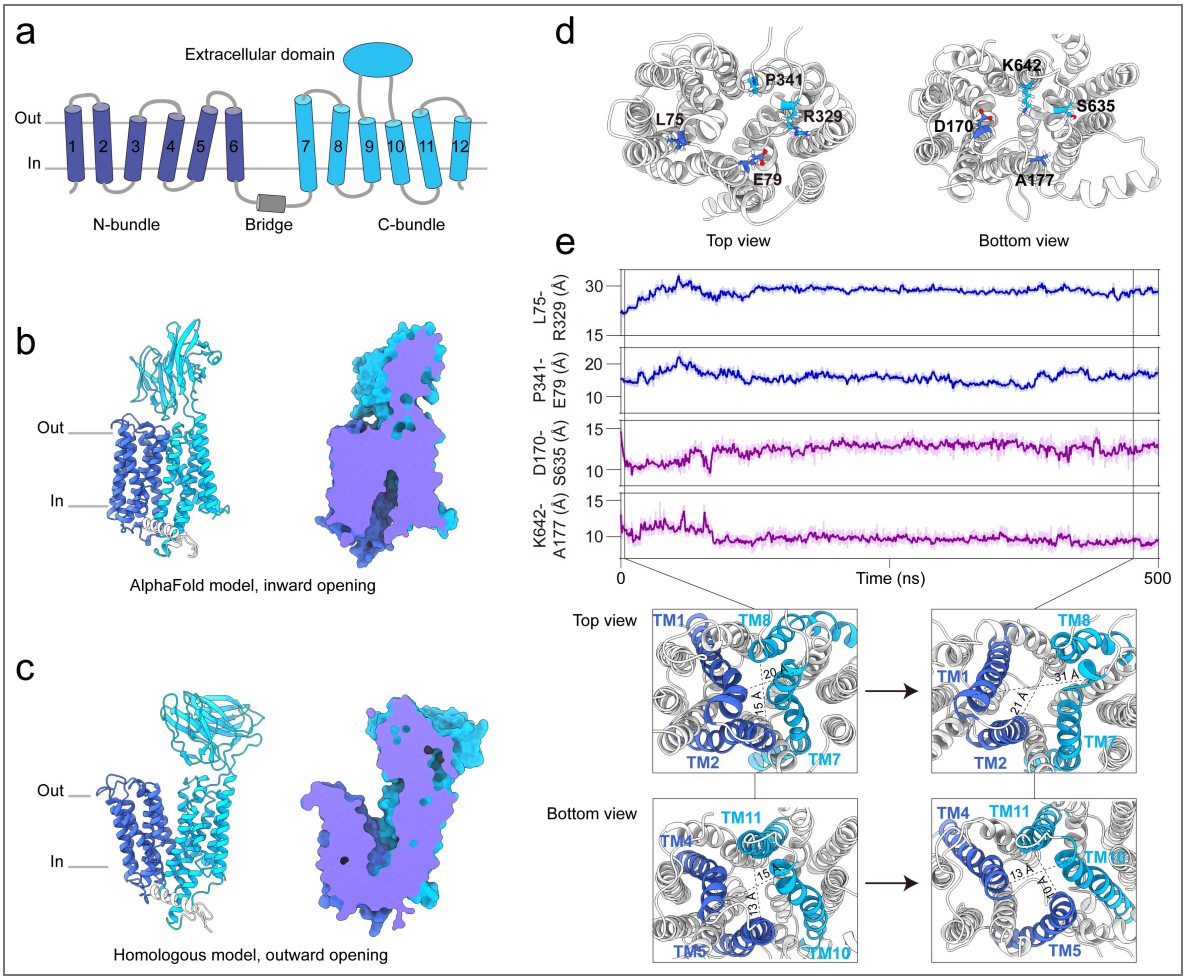

Figure 1. Structural conformations of hPepT2.

(a) The structural toplogy of hPepT2. **(b)** The structural model of hPepT2 built with the AlphaFold approach. **(c)** The structural model of hPepT2 built with the homologous modeling method. The three dimensional structure of rat PepT2 (PDB code: 7NQK) is used as the structural template. **(d)** The residues that are used to define the geometry of the channel of hPepT2. **(e)** The distances between the selected residues and representative structural snapshots are analyzed based on MD simulations.

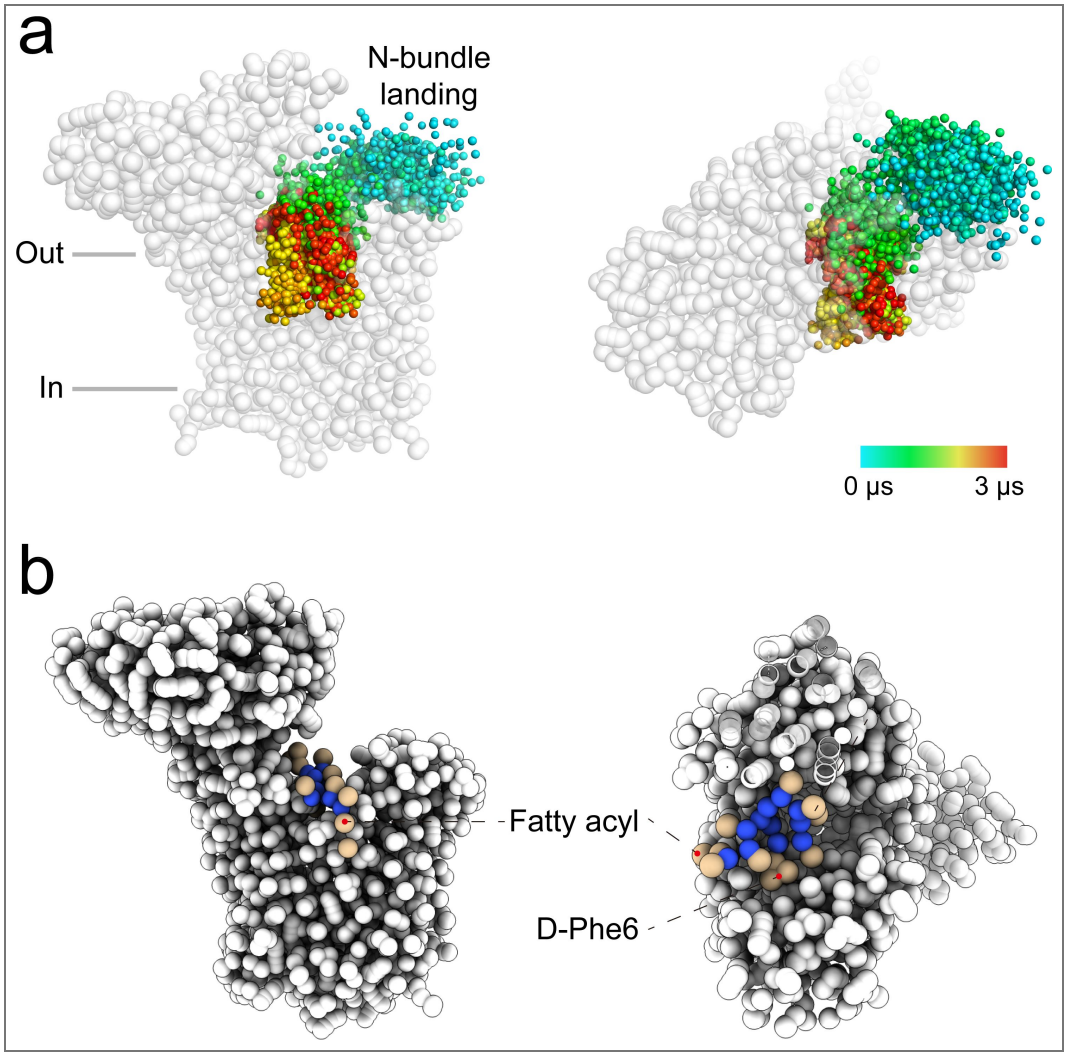

Figure 2. Spontaneous interactions of polymyxin B with hPepT2.

(a) The interaction pathway of polymyxin B with hPepT2. The spatial locations of polymyxin B molecules are represented with colored spheres. The color spectrum from cyan to red indicates the simulation continuity from 0 to 3 μs. **(b)** The equilibrated conformation of hPepT2-polymyxin complex according to the proposed pathway. The polymyxin B molecule is shown in brown and blue spheres with its D-Phe6 and *N*-terminal fatty acyl group labeled.

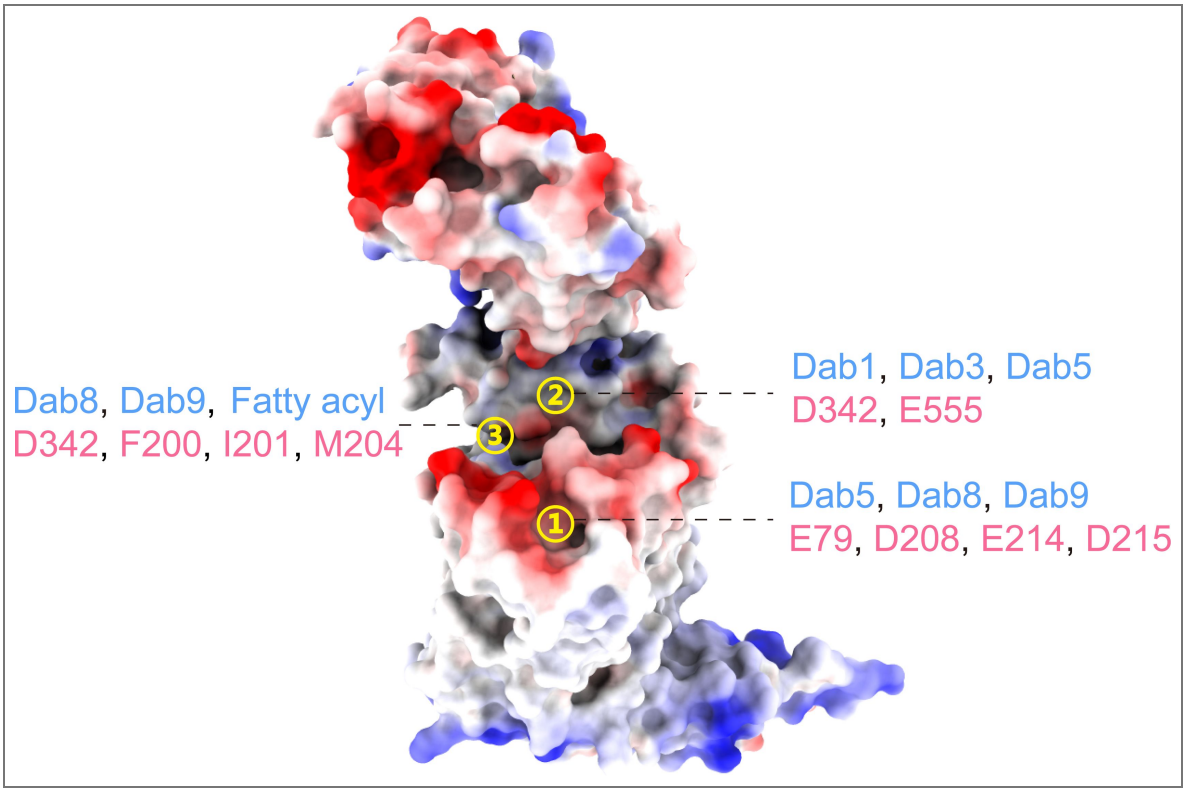

Figure 3. Key structural moieties and residues involved in the interaction of polymyxin B with hPepT2.

The surface potential of hPepT2 is shown with red color indicating negative potential and blue color indicating positive potential.

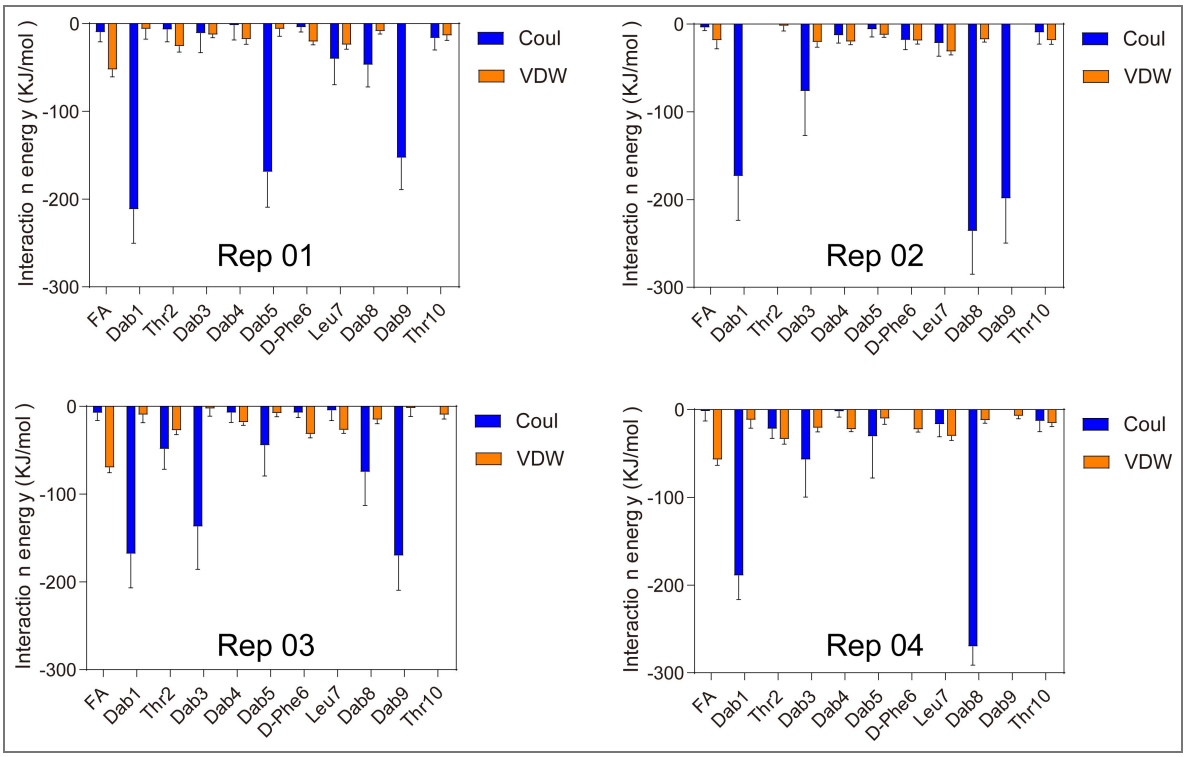

Figure 4. Interaction energy between hPepT2 and each residue of polymyxin B.

The interaction energy was calculated using four MD simulation replicates. **Note:** Coul: electrostatic interaction; VDW: hydrophobic interaction.

proposed residues but also altered their charges from negative to neutral. It is postulated that such a drastic change to the residues of in hPepT2 may largely affect their interactions with polymyxins.

The transport function of these hPepT2 mutants were evaluated as to the uptake of H^3-Gly-Sar (a typical substrate of hPepT2) (11) as well as that of the fluorescent polymyxin probe MIPS-9541 (Fig. 5). The fluorescence images were also captured as the qualitative measurement of the overexpressing cells exposed to our dansyl-fluorescent polymyxin probe MIPS-9541, which indicated the consistent results (Fig. 6). Our data showed that E79A, D80A and D208A mutants maintained the transport activity in the uptake of both substrates. In contrast, E214A, D215A, D342A and E622A mutants had impaired function in the transport of either substrate. Interestingly, D317A and E555A showed differential activity in the uptake of these substrates, suggesting the distinct roles of both residues in the interaction with different substrates.

Subsequently, kinetic analysis was conducted to characterise those hPepT2 mutants with impaired activity in the uptake of MIPS-9541 (i.e. E214A, D215A, D342A and E555A). Noteworthy, the E622A mutant was not included in this analysis due to its critically low transporter function. As shown in Table 1, the D215A mutant demonstrated a doubled K_m (96.6 ± 20.9 μM of D215A *vs.* 47.1 ± 11.9 μM of the wild type) and V_{max} (8610 ± 1363 pmol/(μg/4 min) of D215A *vs.* 4252 ± 652.9 pmol/(μg/4 min) of the wild type). It was also evident that the D342A mutant showed a mildly increased K_m (66.9 ± 13.2 μM of D342A *vs.* 47.1 ± 11.9 μM of the wild type) without altering its V_{max}. The V_{max} values of E214A and E555A were significantly reduced (2332 ± 24.2 pmol/(μg/4 min) of E214A and 2376 ± 320.8 pmol/(μg/4 min) of E555A *vs.* 4252 ± 652.9 pmol/(μg/4 min) of the wild type). However, the K_m values of E214A and E555A mutants were moderately decreased compared to that of the wild type (24.4 ± 4.48 μM of E214A and 26.7 ± 6.99 μM of E555A *vs.* 47.1 ± 11.9 μM of wild type).

Noteworthy, a change of V_{max} value may be due to altered transporter protein expression and/or transporter turnover rate. Thus, the total cell and plasma membrane expression of the hPepT2 and its mutants were investigated to further examine the molecular mechanism underpinning the functional alternations of these mutants. As shown in Fig. 7, E214A, D215A, E555A and E622A significantly reduced total cell expression and cell surface expression. In the case of D342A, it retained the transporter protein expression in the whole cell but had a markedly impaired cell surface expression.

Chemical biology of polymyxin interaction with hPepT2

As described above, the Dab1, Dab3, Dab5, Dab8 and Dab9 residues of polymyxin B were predicted to be involved with its interaction with hPepT2. To test this hypothesis, we designed and synthesised five polymyxin B analogues with substitutions of Alanine on these Dab positions. We performed transport uptake assay to evaluate their interactions with hPepT2. As shown in Fig. 8, the lipopeptide analogues of FADDI-170, FADDI-175, FADDI-793 and FADDI-795 but not FADDI-167 showed reduced uptake in hPepT2 expressing cells, indicating that Dab1, Dab3, Dab5 and Dab9 but not Dab8 are likely involved in the interaction with hPepT2. Therefore, these four lipopeptide analogues may have less intracellular accumulation and reduced nephrotoxicity.

Pharmacological evaluations of lead polymyxin analogues

We firstly assessed the MICs of the four lipopeptide analogues that have disrupted interaction with hPepT2. As shown in Table 2, FADDI-170 showed significantly reduced activity against FADDI-PA025, -EC006, -EC003, -EC001, -AB034 as well as *A. baumannii* ATCC 19606 and ATCC 17978 (MICs increased ≥16 folds, compared to polymyxin B). FADDI-175 displayed low activity against all the tested strains (MICs ≥32 μg/mL), which was not further considered for subsequent testing. FADDI-793 is less active than polymyxin B against *A. baumannii* ATCC 19606, ATCC 17978, FADDI-AB034, -EC006 and -EC003. FADDI-795 was the most active among them, showing comparative MICs against these bacterial strains except for FADDI-PA025, when compared to polymyxin B. Interestingly, FADDI-793 and FADDI-795 were more active than polymyxin B against *K. pneumoniae* ATCC 13883.

Figure 5. Uptake of ^{3}H-Glycosarcosine and polymyxin B fluorescence probe MIPS-9541 by hPepT2 and its mutants.

HEK293 cells were transfected with hPepT2 and its mutant constructs. **(a)** Uptake of ^{3}H-Gly-Sar (5 μM) by hPepT2 or its mutants. **(b)** Uptake of MIPS-9541 (10 μM) by hPepT2 or its mutants. ***$p < 0.001$ *vs.* control by Welch's *t*-test.

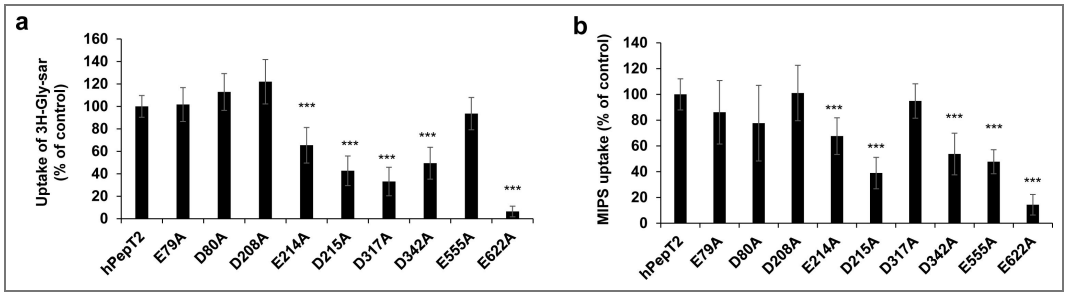

Figure 6. Uptake of polymyxin B fluorescence probe MIPS-9541 in HEK293 cells overexpressing hPepT2 or its mutants by fluorescence imaging.

Note: WT: Wild type; NC: Negative control.

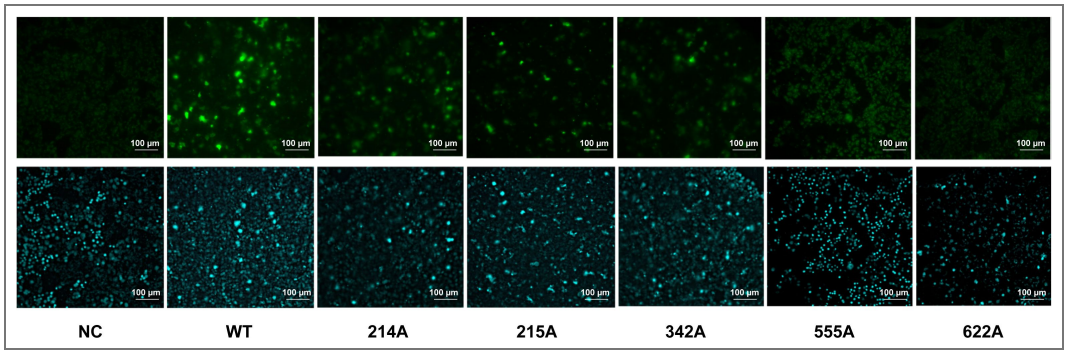

Table 1. Transporter kinetic parameters of MIPS-9541 uptake by hPepT2 and its mutants.

Construct	K_m (μM)	V_{max} (pmol/(μg/4min))
hPepT2	47.1 ± 11.9	4252 ± 652.9
E214A	24.4 ± 4.48	2332 ± 24.2 *
D215A	***96.6 ± 20.9*** *	***8610 ± 1363*** *
D342A	66.9 ± 13.2	4396 ± 583.1
E555A	26.7 ± 6.99	2376 ± 320.8 *

*$p < 0.05$ *vs. control by Welch's t-test*

Figure 7. Total cell and cell surface expression of hPepT2-c-Flag and its mutants.

HEK293 cells were transfected with hPepT2-c-Flag and its mutant constructs. **(a)** Cells were lysed and subject to SDS-electrophoresis. Immunoblots were probed with anti-Flag antibody and then followed by anti-actin antibody. Representative images of each hPepT2 mutant are shown. **(b)** Cell surface proteins were labelled with NHS-ss-Biotin and then pulled down with Streptavidin-agarose beads. Biotin-labelled surface protein samples were subject to SDS-electrophoresis and the immunoblots were probed with anti-Flag antibody. Equal portion of the supernatant samples were separated by SDS-electrophoresis and the immunoblots were incubated with anti-actin antibody. Representative images of each hPeT2 mutant are shown. **(c)** Densitometry analysis of the relative total cell expression of hPepT2 mutants (ratios of Flag/actin). **(d)** Densitometry analysis of the relative cell surface expression of hPepT2 mutants (ratios of Flag/actin). Data are presented as % of the hPepT2 wildtype control (mean ± SD). Experiments were repeated on three occasions. *$p < 0.05$; **$p < 0.01$ *vs.* wildtype control by unpaired *t*-test. Note: WT: wild type; NC: vector-transfected negative control.

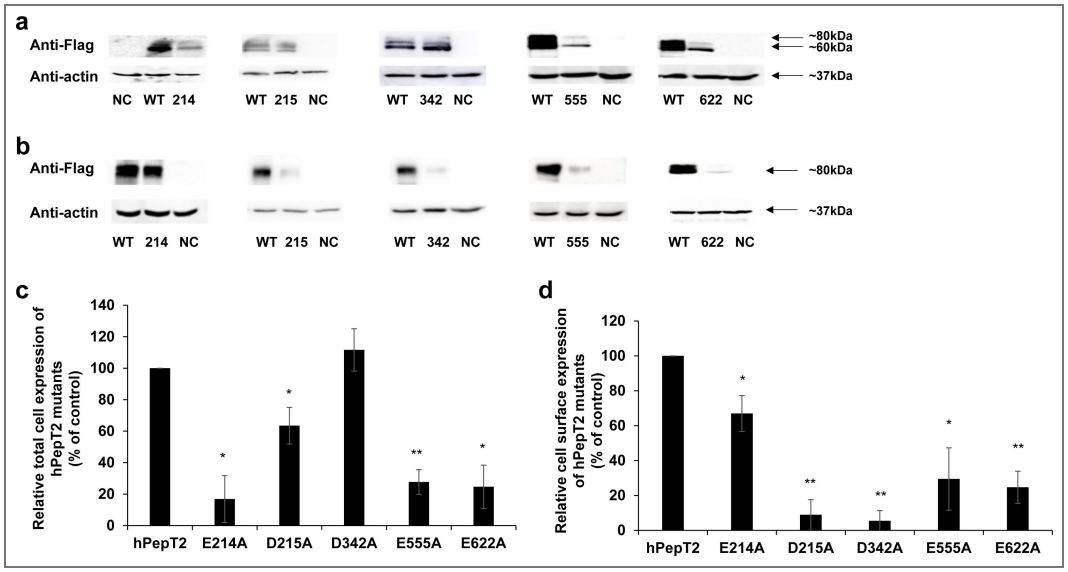

Figure 8. Uptake of polymyxin B fluorescence probe MIPS-9541 and polymyxin analogues by hPepT2.

The data are expressed as the fold of the uptake via hPepT2 *vs.* that of vector transfected control. ***$p < 0.001$ vs. MIPS-9541 control by Welch's *t*-test.

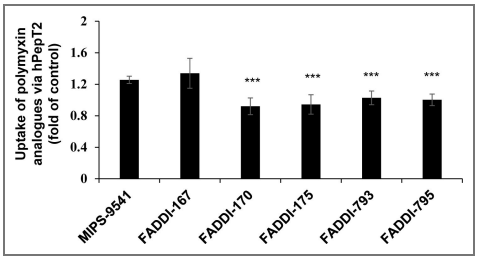

Table 2. Chemical modifications, minimum inhibitory concentrations and nephrotoxicity of polymyxin B (PMB) and its analogues.

Lipopeptide	modification Dab → Ala	Minimum inhibitory concentration (μg/mL)											Max Kidney SQS
		P. aeruginosa ATCC 27853	*FADDI-PA022*	*FADDI-PA025*	*A. baumannii* ATCC 19606	*FADDI-AB034*	[illegible]	*K. pneumoniae* ATCC 13883	*FADDI-KP032*	*FADDI-EC006*	*FADDI-EC001*	*FADDI-EC003*	
PMB		1	1	2	1	0.25	0.5	16	0.5	0.5	0.5	<0.125	+1
FADDI -170	9	2	4	32	>32	>32	32	>32	4	8	8	8	+1
FADDI -175	5	>32	>32	>32	>32	>32	>32	>32	>32	>32	32	32	N.D.
FADDI -793	1	2	4	8	>32	>32	16	4	4	8	2	4	+1
FADDI -795	3	4	8	32	8	4	4	4	1	0.5	1	0.5	0

Polymyxin B was chemically modified at the indicated position by replacing Dab with Ala residue. Lipopeptide was administered to mice via intraperitoneal injection at a dose of 8mg/kg every 2 hr for 6 doses in one day (a total dose of 48 mg/kg/day, n = 3). The kidney histology damage score was determined in the form of Semi-Quantitative Score (SQS): SQS=0, no significant kidney damage; SQS = +1, a mild kidney damage; N.D. not determined.

We then employed the mouse model established in our laboratory to examine the nephrotoxicity of the four antibacterial polymyxin analogues (16). Interestingly, FADDI-795 showed no observable nephrotoxicity; while the other three analogues possess mild kidney toxicity, comparable to polymyxin B (Table 2).

Overall, the transporter uptake study and pharmacological assessments of these polymyxin analogues provide critical mechanistic data on the interaction and transport of polymyxins by hPepT2. Importantly, our integrated computational and cell biology approach highlighted the feasibility to reduce polymyxin nephrotoxicity by disrupting their interactions with hPepT2. Moreover, hPepT2 is a viable target for designing novel polymyxin-like lipopeptide antibiotics with reduced nephrotoxicity.

Discussion

Life-threatening MDR bacterial infections rank among the world's most pressing health threats (17), yet the discovery of antibiotics with novel mechanisms of action has stalled for decades. Polymyxins remain as a last-line therapy for MDR Gram-negative bacterial pathogens, particularly in low to middle income countries; however, their clinical use has been significantly limited due to nephrotoxicity (3, 4).

Our previous study demonstrated that polymyxins are substrates of hPepT2 which mediates the substantial reabsorption of polymyxins in renal proximal tubular cells, leading to nephrotoxicity (11). However, little is known about the interaction between polymyxin molecule and hPepT2. Notably, previous studies have reported that megalin mediates the cellular transport of polymyxins in the kidney via a receptor-mediated endocytosis mechanism (4, 18). Receptor-mediated endocytosis is closely linked to changes in signalling pathways; thus, disrupting the interaction between polymyxins and megalin may lead to unpredictable signalling consequences and complicate treatment outcomes. In contrast, transporter-mediated uptake does not involve such signalling changes, making manipulation of polymyxin-hPepT2 interactions a more favourable strategy for mitigating polymyxin-associated nephrotoxicity. Furthermore, our previous study demonstrated a direct structural interaction of polymyxins with the membrane of human kidney proximal tubular cells (19), showing that polymyxin B inserts its fatty acyl tail into the hydrophobic region of the cell membrane. The stereochemistry at position 3 and the hydrophobicity at positions 6 and 7 of polymyxin B were found to be critical for this interaction. These findings provide important insights into how polymyxins alter membrane dynamics and lipid organization in kidney cells, contributing to a better understanding of polymyxin-induced nephrotoxicity.

The current study developed the first SIR model of polymyxins with hPepT2, expediting the discovery of novel safer lipopeptide antibiotics. We firstly employed MD simulations to predict the binding of polymyxins to hPepT2 (Fig. 1 and 2) and identified several critical amino acid residues of hPepT2 in the recognition of polymyxin molecules. An outward-facing model of hPepT2 was firstly constructed, indicating the access of polymyxin molecules to the lateral opening gate of hPepT2 (Fig. 3). The distinct conformation of polymyxin B indicates that it situates in the central binding cavity of hPepT2. To further explore the conformational change of polymyxin molecules required for hPepT2 transport, all-atom MD simulations were conducted with varying the orientations of polymyxin B. Our results revealed that such a conformation involved a notable flip of polymyxin B enhances the interaction between its fatty acyl chain and the deeper regions of predicted transporter binding pocket of hPepT2. Notably, the subsequent transporter mutagenesis and molecular characterisations of hPepT2 validated our proposed SIR model. Our integrated computational and experimental findings provide the proof-of-concept that disrupting the interaction of polymyxin and hPepT2 is a novel strategy to reduce their nephrotoxicity.

As polymyxins are cationic at physiological pH, we strategically selected the negatively charged amino acids of hPepT2 (i.e. aspartic acid and glutamic acid) for further investigation. The significantly reduced uptake of polymyxin B by hPepT2 mutants E214A, D215A, D342A, E555A and

E622A demonstrated the critical role of these negatively charged residues in transporting polymyxins (Fig. 5 and 6). Moreover, the kinetics results of these transporter mutants elucidated the mechanism underpinning of such functional impairment (Table 1). As both transporter cell surface expression and turn-over rate account for the maximum velocity V_{max} of a transporter protein (10), it was critical to evaluate the protein expression of these transporter mutants in total cell and at cell surface (Fig. 7). Both the kinetic analysis and protein expression profiles (Table 3) showed different mechanisms of impaired polymyxin uptake by hPepT2. For example, it is highly likely that E214A reduced V_{max} due to a reduced total cell and membrane protein expression, while D215A reduced polymyxin uptake mainly due to impaired binding affinity to polymyxins (i.e. increased K_m). Noteworthy, the transporter turnover rate of D215A might increase to compensate for the reduced cell surface expression, thus its V_{max} was overall increased. Similarly, the decreased polymyxin uptake mediated via D342A was primarily attributed to its reduced polymyxin binding affinity, while its decreased membrane protein expression and likely elevated transporter turnover rate resulted in an unchanged V_{max}. In contrast, the dysfunction of E555A was mainly due to its reduced V_{max} likely resulted from a reduced total cell and membrane protein expression, although its binding affinity to polymyxins is slightly increased (i.e. decreased K_m). The kinetic parameters of E622A were unable to be determined due to its low polymyxin uptake and our data indicated that its low protein expression in total cell and at cell surface contributed to its impaired transport activity in polymyxin uptake. Notably, because some transporter mutants (e.g., D342A) exhibited both increased K_m and reduced membrane expression, it is not possible to conclusively determine whether the decreased transporter function results from reduced binding affinity, lower protein expression, or a combination of both, which is a limitation of the current study. Nevertheless, our molecular assay results support the applicability of the bioinformatic predictions, as they allow us to focus the analysis on a limited set of transporter residues that are relevant to our SIR model.

To validate the MD predictions, we further investigated the transport function of these mutant transporters through their uptake of the classic hPepT2 substrate Gly-Sar (Fig. 5A). The uptake of Gly-Sar was dramatically decreased in the mutants of E214A, D215A, D317A, D342A and E622A, which is consistent with the reduced cell surface expression of E214A, D215A, D342A and E622A (Fig. 7). D317A is exceptional as it showed decreased uptake of Gly-Sar but maintained transport function in the case of polymyxin B, which indicated that the residue of D317 is only important for the uptake of Gly-Sar but not polymyxins. E555A is another exception, which remained functional for the uptake of Gly-Sar but reduced uptake of polymyxins. As E555A had a reduced total cell and cell surface expression, its binding affinity to Gly-Sar might increase to compensate for the impaired V_{max}. Thus, the binding pocket of polymyxins does not seem to be identical to that of Gly-Sar. Therefore, the transport inhibition study was only employed as a positive control initially and not considered in the subsequent evaluation of the antibacterial activity of polymyxin analogues.

According to the predicted topology model of hPepT2 (10), E214A and D215A situate at the ECD between TM5 and TM6; D342A resides at the ECD between TM7 and TM8; E555A locates at the ECD between TM9 and TM10; and E622A is within TM10. It was reported that the large ECD between TM9 and TM10 interacts with TM1 to maintain transport function (20). In our study, we demonstrated that E555 residue mildly increased binding affinity to polymyxin B with a reduced V_{max}, likely resulted from the decreased protein expression. These findings highlight the need of more in-depth mechanistic understanding of hPepT2-mediated peptide transport. Notably, E622A in TM10 has a very low transport function in the uptake of polymyxin B, which is largely due to its low protein expression in total cell and on the cell surface (Fig. 5 and 7). Therefore, this residue appears to be essential for preserving hPepT2 stability. Similar findings have been reported in other SLCs (21–23). According to the protein sequence alignment between hPepT2 and another key isoform of SLC15A subfamily, hPepT1, E595 of hPepT1 is the equivalent residue to E622 in hPepT2. It has been shown that the alternation of E595 residue to cysteine substantially impacted on transport function but not protein expression (24). This finding reflects the differing substrate specificities and transport capacities of hPepT1 and hPepT2 (10), highlighting the essential role of hPepT2 in mediating polymyxin transport.Upon validating the predictions of the SIR model of polymyxins and hPepT2, our study was advanced to employ a chemical biology

hPepT2 mutant	K_m	V_{max}	Total cell expression	Cell surface expression
E214A	↓	↓↓	↓↓	↓↓
D215A	↑↑	↑↑	↓↓	↓↓
D342A	↑	*unchanged*	*unchanged*	↓↓
E555A	↓	↓↓	↓↓	↓↓
E622A	N.D.	N.D.	↓↓	↓↓

↓: mildly or moderately decreased; ↓↓: significantly decreased; ↑: mildly or moderately increased; ↑↑: significantly increased; N.D.: not determined.

Table 3. **The kinetic parameters and protein expression profiles of hPepT2 mutant constructs.**

approach to rationally design and in-house synthesize polymyxin analogues. With the hope to interrupt the interaction between hPepT2 and these analogues, we aimed to discover candidate lipopeptide antibiotics with reduced nephrotoxicity while similar or better antibacterial activity. Based on the SIR model, the Dab1, Dab3, Dab5, Dab8 and Dab9 residues of polymyxins are likely to be involved with its interaction with hPepT2 (Fig. 4). Thus, we synthesised FADDI-167, FADDI-170, FADDI-175, FADDI-793 and FADDI-795 with alanine substitutions on these Dab residues. We first examined the hPepT2-mediated uptake of these polymyxin analogues. Interestingly, we discovered that all but not FADDI-167 disrupted the uptake via hPepT2 (Fig. 8). This finding indicated that FADDI-170, FADDI-175, FADDI-793 and FADDI-795 possibly impaired their uptake via hPepT2, thereby leading to reduced accumulation in the kidney and nephrotoxicity. Thus, these four analogues were proceeded for further pharmacological evaluations. Interestingly, FADDI-795 and FADDI-175 showed the best and least antibacterial activity among them, respectively (Table 4). Finally, we employed our mouse model to evaluate the nephrotoxicity of these lipopeptides. Using histological evaluations, FADDI-795 showed no observable toxicity in mouse kidneys and stands out as the lead compound with comparable antibacterial activity. Although beyond this study, FADDI-795 is subject to further pharmacological evaluations, in particular pharmacokinetics in our drug discovery program.

Overall, our study developed the first SIR model of polymyxin with hPepT2 by integrating computational, chemical biology and molecular approaches. Our molecular studies provide strong experimental support for the bioinformatic predictions. Although D215 was the only residue experimentally confirmed to play a key role in polymyxin binding, this insight enabled the targeted design of polymyxin analogues. Subsequent studies of drug efficacy and toxicity demonstrated that FADDI-795 retains antibacterial activity and, importantly, shows reduced nephrotoxicity, highlighting the potential of our approach and underscoring the significance of these findings for drug discovery. Our experimental findings validated the first SIR model and enhanced our understanding of the molecular interaction between the polymyxin molecule and hPepT2. These mechanistic insights are essential for elucidating the clinical dose-limiting nephrotoxicity associated with polymyxin treatment. Moreover, this work serves as a proof-of-concept study, providing the first experimental validation of the predicted polymyxin-hPepT2 binding model. Our ongoing drug discovery efforts will build on these findings to refine the predictive model and accelerate lead optimization for the development of novel, safer lipopeptide antibiotics against Gram-negative bacterial infections.

Materials and Methods

Reagents and chemicals

[^{3}H] glycylsarcosine (Gly-Sar; 2 Ci/μmol) was obtained from BioScientific Pty. Ltd. (Gymea, NSW, Australia). Dulbecco's Modified Eagle Medium (DMEM), fetal bovine serum (FBS), and other culture supplements were purchased from Thermo Scientific (Lidcombe, NSW, Australia). Gly-Sar and polymyxin B1 for molecular studies were bought from Sapphire Biosciences (Redfern, NSW, Australia). Polymyxin B sulfate for animal studies was purchased from BetaPharm (Shanghai, China). MIPS-9541 was synthesised as previously reported (11, 25, 26). Plasmids containing the full-length hPEPT2 and hPepT2-c-Flag were obtained from Australian Biosearch (Balcatta, WA, Australia). All other reagents and chemicals were purchased from Sigma-Aldrich (Castle Hill, NSW, Australia).

Coarse-grained molecular dynamics (MD) simulations

Polymyxin B1 was employed as the prototype (27) and the coarse-grained (CG) model system of hPepT2 was constructed using the Martini Maker module in CHARMM-GUI (28). The membrane lipid composition was 50% phosphatidylcholine, 25% phosphatidylethanolamine and 25% phosphatidylserine (29). In each simulation system, 10 coarse-grained polymyxin molecules were randomly introduced into the simulation system to enhance the binding probability of polymyxin B to hPepT2. These were solvated using CG water particles and neutralised with 0.1 M sodium

Mutant	Forward (5'-3')	Reverse (5'-3')
E79A	atatagatgtggaggtatctgcattccagtgcaggaaatac	gtatttcctgcactggaatgcagatacctccacatc tatat
D80A	cctgcactggaatgaagctacctccacatctatatacc	ggtatatagatgtggaggtagcttcattccagtgca gg
D208A	gggtacgactctcctcgacacgttacaaaacc	cccatgctgagaggagctgtgcaatgttttgg
E214A	gccaatgcatagcagtctgctccaaaacattgcacat	atgtgcaatgttttggagcagactgctatgcattgg c
D215A	aaaagccaatgcatagcaggcttctccaaaacattgcac	gtgcaatgttttggagaagcctgctatgcattggct ttt
D317A	cccgagaaaaccgagtcgtcccaagtgc	gggctcttttggctcagcagggttcacg
D342A	gtgcttcagccggcccagatgcaggttc	gaacctgcatctgggccggctgaagcac
E555A	gtgcactgcagggtatgctcctctttgcacagt	actgtgcaaagaggagcataccctgcagtgcac
E622A	gacagagaacatgaccgccccagctgtaaccag	ctggttacagctggggcggtcatgttctctgtc

Table 4. **Primers used for hPepT2 mutagenesis**

chloride in a 15 × 15 × 14 nm^3 simulation box. All CG simulations were conducted under periodic boundary conditions using the GROMACS program (version 2021.2) and Martini 2.2 force field (30, 31). To eliminate steric interference, the steepest energy minimization was performed for every system to give the maximum force below 1,000 kJ mol^{-1} nm^{-2}. Subsequently, a six-step equilibration cycle was carried out by gradually turning off the position restraints on the lipid and polymyxin molecules. Finally, 3μs-production simulations with two replicates were conducted for each system in the NPT (referring to the number of particles (N), system pressure (P) and temperature (T)) ensemble. The temperature and pressure were coupled to 310 K using the velocity rescaling method (time constant of 1 ps) and 1 bar using the semi-isotropic barostat and Parrinello-Rahman algorithm (time constant of 5 ps), respectively (32).

All-atom MD simulations

The previous study of $PepT_{Xc}$, a homolog of hPepT2, revealed that the protonation of its His67 promotes the outward opening conformation (33), therefore the corresponding residue His87 of hPepT2 was set to be protonated during all-atom simulations to bias toward an outward opening state. In the two CGMD replicates, polymyxin B eventually bound to the lateral opening gate of hPepT2. To examine the detailed interaction between polymyxin and hPepT2, a single polymyxin B molecule was introduced to the binding pocket of hPepT2 using Autodock Vina (34). Furthermore, to enhance the sampling of the binding dynamics, four different poses of polymyxin B were employed to build the initial hPepT2-polymyxin complex. Then, the membrane protein system of hPepT2-polymyxin was constructed using the membrane builder module in CHARMM-GUI (35).

GROMACS 2021.2 was used to perform all MD simulations with the CHARMM36 all-atom force field (36). A time step of 2 fs was employed to integrate the Newtonian equations of motion and all bonds involving hydrogen atoms were constrained. Long-range electrostatic interactions were treated using the Particle Mesh Ewald (PME) method with a switching function applied between 10 and 12 Å (37). After energy minimization, the system was equilibrated through a series of MD simulation steps in the NVT (referring to the number of particles (N), system volume (V) and temperature (T)) and NPT ensembles (310 K, 1 bar), during which positional restraints on membrane and protein atoms were gradually reduced. The root mean square deviations of polymyxin B were calculated to examine the simulation equilibration (Fig. S1). No restraints were applied in the final stage of equilibration and throughout the production run. The PME method was employed to treat long-range electrostatic interactions with a short-range cut-off of 1.2 nm, while the shifted Lennard–Jones potential algorithm was used to calculate Van der Waals interactions with a general cut-off of 1.2 nm and a shifting cut-off of 1.0 nm (38, 39). The trajectory during production simulations was recorded every 10 ps.

Site-directed mutagenesis and plasmid DNA sequencing

The hPepT2 mutants were generated using a QuickChange II site-directed mutagenesis kit (Agilent Technologies, Mulgrave, Victoria, Australia) with the primers listed in Table 4. All mutant construct sequences were confirmed by DNA sequencing (Ramaciotti Centre for Gene Function Analysis, Randwick, NSW, Australia) with the Bigdye™ Terminator v3.1 kit (Thermo Scientific, Lidcombe, NSW, Australia) (9, 21, 40–42).

Transfection of hPepT2 and its mutants into HEK293 cells

HEK293 cells were cultured in DMEM supplemented with 10% FBS at 37°C with 5% CO_2. Cells were transfected with hPepT2 or its mutant plasmid DNA using Lipofectamine 2000 Reagent as to the manufacture's instruction (Invitrogen, Mount Waverley, VIC, Australia) (7, 11, 43–45). At 24 h after transfection, the cellular uptake of [^{3}H] Gly-Sar or MIPS-9541 was assessed.

Transport uptake assay

To evaluate the uptake of [^{3}H] Gly-Sar via hPepT2 or its mutant transporters, we measured the accumulation of [^{3}H] Gly-Sar in over-expressing HEK293 cells. The uptake was conducted at 37°C in phosphate-buffered saline (PBS, pH 5.0) containing 5 mM glucose. The specific substrate

concentration was 2.5 μM [^{3}H] Gly-Sar and the duration was 8 min according to our previous studies (7, 11). The uptake assay was terminated by three rapid washes with ice-cold PBS. Samples were lysed in 0.2 M NaOH, neutralized in 0.2 M HCL and then processed for liquid scintillation counting. The uptake counts for hPepT2 or its mutant expressing cells were all subtracted with that of the control.

To evaluate the uptake of polymyxin B via hPepT2 or its mutant transporters, we measured the accumulation of a validated fluorescent polymyxin probe MIPS-9541 and polymyxin analogues (i.e. FADDI-167, -170, -175, -793 and -795, Fig. S2) in over-expressing HEK293 cells (11). The uptake was performed in PBS (pH 5.0) supplemented with 5 mM glucose for 10 min at 37°C. Intracellular fluorescence accumulation was quantified with excitation/emission wavelengths of 350 nm / 518 nm using a Tecan Safire II microplate reader (Thermo Scientific, Lidcombe, NSW, Australia). Background counts of the vector-transfected cells were subtracted from all uptake measurements. Kinetic analysis was conducted by measuring the uptake of transporter expressing cells with a range of concentrations of MIPS-9541 (0 - 50 μM) over 10 min. Apparent K_m and V_{max} values were determined using GraphPad Prism 10.0 (11, 46).

Fluorescence imaging of MIPS-9541

HEK293 cells were seeded on chamber slides and transfected with hPepT2 or its mutant plasmids. After 24 h, culture medium was removed and cells were incubated with freshly prepared MIPS-9541 solution in PBS (10 μM, pH 5.0) for 10 min at 37°C. Cells were then washed with ice-cold PBS for three times and mounted in SlowFade Gold Antifade Mountant reagent supplemented with 4',6-diamidino-2-phenylindole (DAPI, Thermo Scientific, Lidcombe, NSW, Australia). Samples were imaged with a Leica Thunder 3D Imager (Leica Microsystems, North Ryde, NSW, Australia).

Cell surface biotinylation

We employed sulfo-NHS-SS-Biotin to label the plasma membrane protein in HEK293 cells overexpressing hPepT2 or its mutants (47). Cell culture plates were pre-chilled on ice. Culture medium was aspirated, and cells were washed twice with cold PBS (pH 8.0). Freshly prepared 1 mg/mL Sulfo-NHS-SS-Biotin in PBS (pH 8.0) was then added to each well and incubated for 30 min. Cells were washed twice with 100 mM glycine in PBS (pH 8.0) and then three times with PBS (pH 7.4). Cells were lysed in the lysis buffer (Tris 10 mM, NaCl 150 mM, EDTA 1 mM, SDS 0.1% and Triton X-100 1% with 1:1,000 dilution of a protease inhibitor cocktail) (21). Cell lysate was subject to centrifugation at 14,000 *g* and 4°C for 10 min and the supernatant was collected. Pre-washed Streptavidin-Agarose beads were supplied to the samples with rotating at 4°C for 1 h. After three rounds of centrifugation and washing with PBS (pH 7.4), beads were resuspended in PBS with 1x Laemmli buffer containing 2.5% β-mercaptoethanol and incubated at 55°C for 30 min. The remaining supernatant was collected, denatured and subject to electrophoresis.

Total cell lysis, electrophoresis and immunoblotting

Upon washing, cells were collected and lysed in the lysis buffer. After incubating on ice for 10 min, cell lysate was centrifugated at 14,000 *g* and 4°C for 10 min. The supernatant was collected as total cell lysate and denatured at 55°C in 1x Laemmli buffer containing 2.5% β-mercaptoethanol for 30 min.

Protein lysate samples were loaded to 10% SDS-PAGE gels followed with electrophoresis as described before (48) and the protein samples on the gels were transferred to polyvinylidene difluoride (PVDF) membranes. Following blocking with 5% non-fat milk in PBS-Tween (Na_2HPO_4 80 mM, KH_2PO_4 20 mM, NaCl 100 mM, and 0.05% Tween 20, pH 7.5) and multiple washing with PBS-Tween, the immunoblots were incubated at 4°C overnight with anti-flag (DYKDDDDK) antibody (1:1,000; Catalogue Number 2368, Genesearch, Arundel, QLD, Australia) or anti-β-actin antibody (1:2,000, Catalogue Number 4967, Genesearch). After washing with PBS-Tween for three times, the immunoblots were incubated at room temperature for 1 h with goat anti-rabbit IgG conjugated with HRP (1:5,000; Catalogue Number A0545, Sigma-Aldrich) or goat anti-mouse IgG conjugated with HRP (1:10,000; Catalogue Number A2554, Sigma Aldrich). The blots were washed,

incubated with Immobilon Western Chemiluminescent HRP substrate (Merck Millipore, Kilsyth, VIC, Australia) and imaged with an ImageQuant LAS 500 (GE healthcare, Avantor, PA, USA). The densitometry analysis of immunoblots was processed with Image J (NIH, Bethesda, MD, USA).

Chemical synthesis of polymyxin analogues

Five lipopeptides (FADDI-167, FADDI-170, FADDI-175, FADDI-793 and FADDI-795) were synthesised and purified in house as described before (16, 49). Briefly, the lipopeptides were prepared using a Protein Technologies Prelude automated peptide synthesizer as to the standard protocol of Fmoc solid-phase peptide chemistry.

Measurements of minimum inhibitory concentrations (MICs)

MICs were measured using the broth micro-dilution method with clinical isolates and American Type Culture Collection (ATCC) strains (50). Each bacterial strain (~10^6 colony forming units per mL) was suspended in 100 µL of freshly prepared cation-adjusted Mueller-Hinton broth (CaMHB) in 96-well plates. Lipopeptides were diluted into different concentrations in CaMHB and added to the plates for subsequent incubation at 37°C for 18-24 h. MICs were determined as the lowest concentration that the visible growth of bacteria was inhibited.

Nephrotoxicity in mice

The mouse nephrotoxicity study was approved by the Monash Animal Ethics Committee. Mice were maintained in micro-isolators in a temperature-controlled PC2 animal laboratory with an ambient humidity of 50-70% and a 12 h/12 h dark/light cycle. Lipopeptide solutions were subcutaneously administered to mice with a dose of 8 mg/kg every 2 h for 6 doses in one day (a total dose of 48 mg/kg/day). At 24 h after the last injection, mice were sacrificed, the kidneys were collected from mice immediately and fixed in 10% formalin buffer (pH 7.4, Sigma Aldrich, Australia). Histological examination of the kidney samples was conducted at the Australian Phenomics Network-Histopathology and Organ Pathology (University of Melbourne, Parkville, VIC, Australia). An experienced pathologist, who was blind to the treatment, rated the histology and severity of the nephrotoxicity as to three grades with scores 1 to 10 (16). The percentage of kidney affected was also scaled in the range of 0-6 (0: <1%; 1: 1 to<5%; 2: 5 to <10%; 3: 10 to <20%; 4: 20 to<30%; 5: 30 to ≤ 40% and 6: >40%). A semi-quantitative score (SQS) was calculated using the grade score and kidney damage percentage to quantify the overall kidney damage (16).

Statistical analyses

Unpaired *t*-test was employed to detect the variance between the protein expression of hPepT2 and its mutants. Welch's *t*-test was used to assess the differences between the transport function or kinetic parameters of hPepT2 and its mutants. All data are expressed as mean ± standard deviation (SD) with a p value of <0.05 considered as statistically significant. All experiments were repeated three times with triplicates in each experiment.

Data availability

All data are available upon request.

Additional information

Ethics approval and consent to participate

This study was approved by the Monash Animal Ethics Committee.

Author Contributions

XJ, JL and FZ conceived the project, XJ, YL, MAA, KDR and FZ performed the computational, chemical biology and molecular experiments, XJ, YL, LX, JL and FZ analysed the data, XJ, YL and FZ drafted the manuscript, MX, LW, TV, KDR, VT, QTZ and JL critically reviewed and revised the

manuscript.

Funding

We acknowledge the funding support of e-Asia Joint Research Program (2018589). XJ is supported by the National Natural Science Foundation of China (32401034 and 32301041), Basic Research Program of Jiangsu (BK20240425), Shandong Excellent Young Scientists (Overseas) Fund Program (2023HWYQ-044). VT is supported by the Program Management Unit B (Brain Power, Manpower), Ministry of Higher Education, Science, Research and Innovation, Thailand.

Abbreviations

ATCC: American Type Culture Collection
CaMHB: cation-adjusted Mueller-Hinton broth
CG: coarse-grained
Coul: electrostatic interaction
Cryo-EM: Cryo-electron microscopy
DAPI: 4′,6-diamidino-2-phenylindole
DMEM: Dulbecco's Modified Eagle Medium
ECD: extracellular domain
FBS: fetal bovine serum
Gly-Sar: glycosarcosine
hPepT2: human oligopeptide transporter 2
MD: molecular dynamics
MDR: multidrug-resistant
MIC: minimum inhibitory concentration
NPT: number of particles, system pressure and temperature
NVT: number of particles, system volume and temperature
PBS: phosphate-buffered saline
PME: Particle Mesh Ewald
PVDF: polyvinylidene difluoride
SD: standard deviation
SIR: structure-interaction relationship
SLCs: solute carrier transporters
SQS: semi-quantitative score
TM: transmembrane domain
VDW: hydrophobic interaction.

Funding

Funder	Grant reference number	Author
e-Asia Joint Research Program	2018589	Xukai Jiang Fanfan Zhou Qi Tony Zhou Visanu Thamlikitkul Jian Li
MOST | National Natural Science Foundation of China (NSFC)	32401034	Xukai Jiang
MOST | National Natural Science Foundation of China (NSFC)	32301041	Xukai Jiang
JST | Jiangsu Natural Science Foundation | Basic Research Program of Jiangsu Province	BK20240425	Xukai Jiang
Shandong Excellent Young Scientists (Overseas) Fund Program, China	2023HWYQ-044	Xukai Jiang

Program Management Unit B (Brain Power, Manpower), Ministry of Higher Education, Science, Research and Innovation, Thailand	Visanu Thamlikitkul

Author ORCID iDs

Xukai Jiang: https://orcid.org/0000-0002-3624-8732
Fanfan Zhou: https://orcid.org/0000-0002-1982-1541
Jian Li: https://orcid.org/0000-0001-7953-8230

Author notes

Competing interests: JL, TV, and KDR are listed as inventors on the patent application WO2015149131 'Polymyxin Derivatives as Antimicrobial Compounds' which covers new-generation polymyxins and has been licensed to Qpex Biopharma and Brii Biosciences. JL received grants, speaking honoraria, and consulting fees from Northern Antibiotics, Avexa, Genentech, Healcare, CTTQ, Aosaikang, Jiayou Medicine, MedCom, Fansheng Biotech, DanDi BioScience, Qpex Biopharma, and Xellia Pharmaceuticals. JL is CEO of Sliabx Pharmaceuticals and Cinfinno Biotech and holds equities in both companies. All other authors declare no conflict of interest.

Additional files

Supplementary file 1. Supporting information.

References

1. **Morehead MS,** Scarbrough C (2018) Emergence of global antibiotic resistance. *Prim Care* **45**:467-84 https://doi.org/10.1016/j.pop.2018.05.006 | PubMed
2. **Baindara P,** Kumari S, Dinata R, Mandal SM (2025) Antimicrobial peptides: evolving soldiers in the battle against drug-resistant superbugs. *Mol Biol Rep* **52**:432 https://doi.org/10.1007/s11033-025-10533-z | PubMed
3. **Nang SC,** Azad MAK, Velkov T, Zhou QT, Li J (2021) Rescuing the last-line polymyxins: achievements and challenges. *Pharmacol Rev* **73**:679-728 https://doi.org/10.1124/pharmrev.120.000020 | PubMed
4. **Azad MAK,** Nation RL, Velkov T, Li J (2019) Mechanisms of polymyxin-induced nephrotoxicity. *Adv Exp Med Biol* **1145**:305-19 https://doi.org/10.1007/978-3-030-16373-0_18 | PubMed
5. **Wang JL,** Xiang BX, Song XL, Que RM, Zuo XC, Xie YL (2022) Prevalence of polymyxin-induced nephrotoxicity and its predictors in critically ill adult patients: A meta-analysis. *World J Clin Cases* **10**:11466-85 https://doi.org/10.12998/wjcc.v10.i31.11466 | PubMed
6. **Slingerland CJ,** Martin NI (2024) Recent advances in the development of polymyxin antibiotics: 2010-2023. *ACS Infect Dis* **10**:1056-79 https://doi.org/10.1021/acsinfecdis.3c00630 | PubMed
7. **Lu X,** Chan T, Zhu L, Bao X, Velkov T, Zhou QT, et al. (2018) The inhibitory effects of eighteen front-line antibiotics on the substrate uptake mediated by human Organic anion/cation transporters, Organic anion transporting polypeptides and Oligopeptide transporters in in vitro models. *Eur J Pharm Sci* **115**:132-43 https://doi.org/10.1016/j.ejps.2018.01.002 | PubMed
8. **Zhou F,** Zhu L, Wang K, Murray M (2017) Recent advance in the pharmacogenomics of human Solute Carrier Transporters (SLCs) in drug disposition. *Adv Drug Deliv Rev* **116**:21-36 https://doi.org/10.1016/j.addr.2016.06.004 | PubMed
9. **Chan T,** Lu X, Shams T, Zhu L, Murray M, Zhou F (2016) The role of N-glycosylation in maintaining the transporter activity and expression of human oligopeptide transporter 1. *Mol Pharm* **13**:3449-56 https://doi.org/10.1021/acs.molpharmaceut.6b00462 | PubMed
10. **Luo Y,** Gao J, Jiang X, Zhu L, Zhou QT, Murray M, et al. (2023) Molecular insights to the structure-interaction relationships of human proton-coupled oligopeptide transporters (PepTs). *Pharmaceutics* **15** https://doi.org/10.3390/pharmaceutics15102517 | PubMed

11. **Lu X,** Chan T, Xu C, Zhu L, Zhou QT, Roberts KD, et al. (2016) Human oligopeptide transporter 2 (PEPT2) mediates cellular uptake of polymyxins. *J Antimicrob Chemother* **71**:403-12 https://doi.org/10.1093/jac/dkv340 | PubMed

12. **Ocheltree SM,** Shen H, Hu Y, Xiang J, Keep RF, Smith DE (2004) Role of PEPT2 in the choroid plexus uptake of glycylsarcosine and 5-aminolevulinic acid: studies in wild-type and null mice. *Pharm Res* **21**:1680-5 https://doi.org/10.1023/b:pham.0000041465.89254.05 | PubMed

13. **Smith DE,** Clemencon B, Hediger MA (2013) Proton-coupled oligopeptide transporter family SLC15: physiological, pharmacological and pathological implications. *Mol Aspects Med* **34**:323-36 https://doi.org/10.1016/j.mam.2012.11.003 | PubMed

14. **Zhao D,** Lu K (2015) Substrates of the human oligopeptide transporter hPEPT2. *Biosci Trends* **9**:207-13 https://doi.org/10.5582/bst.2015.01078 | PubMed

15. **Parker JL,** Deme JC, Wu Z, Kuteyi G, Huo J, Owens RJ, et al. (2021) Cryo-EM structure of PepT2 reveals structural basis for proton-coupled peptide and prodrug transport in mammals. *Sci Adv* **7** https://doi.org/10.1126/sciadv.abh3355 | PubMed

16. **Roberts KD,** Zhu Y, Azad MAK, Han ML, Wang J, Wang L, et al. (2022) A synthetic lipopeptide targeting top-priority multidrug-resistant Gram-negative pathogens. *Nat Commun* **13**:1625 https://doi.org/10.1038/s41467-022-29234-3 | PubMed

17. **Li J,** Nation RL, Turnidge JD, Milne RW, Coulthard K, Rayner CR, et al. (2006) Colistin: the re-emerging antibiotic for multidrug-resistant Gram-negative bacterial infections. *Lancet Infect Dis* **6**:589-601 https://doi.org/10.1016/s1473-3099(06)70580-1 | PubMed

18. **Abdelraouf K,** Chang KT, Yin T, Hu M, Tam VH (2014) Uptake of polymyxin B into renal cells. *Antimicrob Agents Chemother* **58**:4200-2 https://doi.org/10.1128/aac.02557-14 | PubMed

19. **Jiang X,** Zhang S, Azad MAK, Roberts KD, Wan L, Gong B, et al. (2020) Structure-Interaction Relationship of Polymyxins with the Membrane of Human Kidney Proximal Tubular Cells. *ACS Infect Dis* **6**:2110-9 https://doi.org/10.1021/acsinfecdis.0c00190 | PubMed

20. **Shen J,** Hu M, Fan X, Ren Z, Portioli C, Yan X, et al. (2022) Extracellular domain of PepT1 interacts with TM1 to facilitate substrate transport. *Structure* **30**:1035-41. https://doi.org/10.1016/j.str.2022.04.011 | PubMed

21. **Chan T,** Zheng J, Zhu L, Grewal T, Murray M, Zhou F (2015) Putative transmembrane domain 6 of the human organic anion transporting polypeptide 1A2 (OATP1A2) influences transporter substrate binding, protein trafficking, and quality control. *Mol Pharm* **12**:111-9 https://doi.org/10.1021/mp500459b | PubMed

22. **Hong M,** Li S, Zhou F, Thomas PE, You G (2010) Putative transmembrane domain 12 of the human organic anion transporter hOAT1 determines transporter stability and maturation efficiency. *J Pharmacol Exp Ther* **332**:650-8 https://doi.org/10.1124/jpet.109.160515 | PubMed

23. **Hong M,** Zhou F, Lee K, You G (2007) The putative transmembrane segment 7 of human organic anion transporter hOAT1 dictates transporter substrate binding and stability. *J Pharmacol Exp Ther* **320**:1209-15 https://doi.org/10.1124/jpet.106.117663 | PubMed

24. **Xu L,** Haworth IS, Kulkarni AA, Bolger MB, Davies DL (2009) Mutagenesis and cysteine scanning of transmembrane domain 10 of the human dipeptide transporter. *Pharm Res* **26**:2358-66 https://doi.org/10.1007/s11095-009-9952-9 | PubMed

25. **Deris ZZ,** Swarbrick JD, Roberts KD, Azad MA, Akter J, Horne AS, et al. (2014) Probing the penetration of antimicrobial polymyxin lipopeptides into gram-negative bacteria. *Bioconjug Chem* **25**:750-60 https://doi.org/10.1021/bc500094d | PubMed

26. **Yun B,** Azad MA, Nowell CJ, Nation RL, Thompson PE, Roberts KD, et al. (2015) Cellular uptake and localization of polymyxins in renal tubular cells using rationally designed fluorescent probes. *Antimicrob Agents Chemother* **59**:7489-96 https://doi.org/10.1128/aac.01216-15 | PubMed

27. **Jiang X,** Sun Y, Yang K, Yuan B, Velkov T, Wang L, et al. (2021) Coarse-grained simulations uncover Gram-negative bacterial defense against polymyxins by the outer membrane. *Comput Struct Biotechnol J* **19**:3885-91 https://doi.org/10.1016/j.csbj.2021.06.051 | PubMed

28. **Qi Y,** Ingolfsson HI, Cheng X, Lee J, Marrink SJ, Im W (2015) CHARMM-GUI martini maker for coarse-grained simulations with the martini force field. *J Chem Theory Comput* **11**:4486-94 https://doi.org/10.1021/acs.jctc.5b00513 | PubMed

29. **Vance JE** (2008) Phosphatidylserine and phosphatidylethanolamine in mammalian cells: two metabolically related aminophospholipids. *J Lipid Res* **49**:1377-87 https://doi.org/10.1194/jlr.r700020-jlr200 | PubMed

30. **Van Der Spoel D,** Lindahl E, Hess B, Groenhof G, Mark AE, Berendsen HJ (2005) GROMACS: fast, flexible, and free. *J Comput Chem* **26**:1701-18 https://doi.org/10.1002/jcc.20291 | PubMed

31. **Qi Y,** Cheng X, Han W, Jo S, Schulten K, Im W (2014) CHARMM-GUI PACE CG builder for solution, micelle, and bilayer coarse-grained simulations. *J Chem Inf Model* **54**:1003-9 https://doi.org/10.1021/ci500007n | PubMed

32. **Parrinello M,** Rahman A (1981) Polymorphic transitions in single-crystals - a new molecular-dynamics method. *J Appl Phys* **52**:7182-90 https://doi.org/10.1063/1.328693

33. **Parker JL,** Li C, Brinth A, Wang Z, Vogeley L, Solcan N, et al. (2017) Proton movement and coupling in the POT family of peptide transporters. *Proc Natl Acad Sci U S A* **114**:13182-7 https://doi.org/10.1073/pnas.1710727114 | PubMed

34. **Forli S,** Huey R, Pique ME, Sanner MF, Goodsell DS, Olson AJ (2016) Computational protein-ligand docking and virtual drug screening with the AutoDock suite. *Nat Protoc* **11**:905-19 https://doi.org/10.1038/nprot.2016.051 | PubMed

35. **Park S,** Choi YK, Kim S, Lee J, Im W (2021) CHARMM-GUI membrane builder for lipid nanoparticles with ionizable cationic lipids and PEGylated lipids. *J Chem Inf Model* **61**:5192-202 https://doi.org/10.1021/acs.jcim.1c00770 | PubMed

36. **Lee J,** Cheng X, Swails JM, Yeom MS, Eastman PK, Lemkul JA, et al. (2016) CHARMM-GUI input generator for NAMD, GROMACS, AMBER, OpenMM, and CHARMM/OpenMM simulations using the CHARMM36 additive force field. *J Chem Theory Comput* **12**:405-13 https://doi.org/10.1021/acs.jctc.5b00935 | PubMed

37. **Darden T,** York D, Pedersen L (1993) Particle mesh ewald - an N.Log(N) method for ewald sums in large systems. *J Chem Phys* **98**:10089-92 https://doi.org/10.1063/1.464397

38. **de Souza ON,** Ornstein RL (1997) Effect of periodic box size on aqueous molecular dynamics simulation of a DNA dodecamer with particle-mesh Ewald method. *Biophys J* **72**:2395-7 https://doi.org/10.1016/s0006-3495(97)78884-2 | PubMed

39. **Huang C,** Choi PY, Kostiuk LW (2011) A method for creating a non-equilibrium NT(P1-P2) ensemble in molecular dynamics simulation. *Phys Chem Chem Phys* **13**:20750-9 https://doi.org/10.1039/c1cp21492f | PubMed

40. **Zheng J,** Chan T, Cheung FS, Zhu L, Murray M, Zhou F (2014) PDZK1 and NHERF1 regulate the function of human organic anion transporting polypeptide 1A2 (OATP1A2) by modulating its subcellular trafficking and stability. *PLoS One* **9**:e94712 https://doi.org/10.1371/journal.pone.0094712 | PubMed

41. **Zhou F,** Zheng J, Zhu L, Jodal A, Cui PH, Wong M, et al. (2013) Functional analysis of novel polymorphisms in the human SLCO1A2 gene that encodes the transporter OATP1A2. *AAPS J* **15**:1099-108 https://doi.org/10.1208/s12248-013-9515-1 | PubMed

42. **Zhou F,** Zhu L, Cui PH, Church WB, Murray M (2010) Functional characterization of nonsynonymous single nucleotide polymorphisms in the human organic anion transporter 4 (hOAT4). *Br J Pharmacol* **159**:419-27 https://doi.org/10.1111/j.1476-5381.2009.00545.x | PubMed

43. **Ali Y,** Shams T, Cheng Z, Li Y, Chun CS, Shu W, et al. (2021) Impaired transport activity of human Organic anion transporters (OATs) and Organic anion transporting polypeptides (OATPs) by Wnt inhibitors. *J Pharm Sci* **110**:914-24 https://doi.org/10.1016/j.xphs.2020.10.009 | PubMed

44. **Chan T,** Cheung FS, Zheng J, Lu X, Zhu L, Grewal T, et al. (2016) Casein kinase 2 is a novel regulator of the human Organic anion transporting polypeptide 1A2 (OATP1A2) trafficking. *Mol Pharm* **13**:144-54 https://doi.org/10.1021/acs.molpharmaceut.5b00576 | PubMed

45. **Li Z,** Cheung FS, Zheng J, Chan T, Zhu L, Zhou F (2014) Interaction of the bioactive flavonol, icariin, with the essential human solute carrier transporters. *J Biochem Mol Toxicol* **28**:91-7 https://doi.org/10.1002/jbt.21540 | PubMed

46. **Chan T,** Zhu L, Madigan MC, Wang K, Shen W, Gillies MC, et al. (2015) Human organic anion transporting polypeptide 1A2 (OATP1A2) mediates cellular uptake of all-trans-retinol in human retinal pigmented epithelial cells. *Br J Pharmacol* **172**:2343-53 https://doi.org/10.1111/bph.13060 | PubMed

47. **Zhou F,** Hong M, You G (2007) Regulation of human organic anion transporter 4 by progesterone and protein kinase C in human placental BeWo cells. *Am J Physiol Endocrinol Metab* **293**:E57-61 https://doi.org/10.1152/ajpendo.00696.2006 | PubMed

48. **Zhou F,** Xu W, Tanaka K, You G (2008) Comparison of the interaction of human organic anion transporter hOAT4 with PDZ proteins between kidney cells and placental cells. *Pharm Res* **25**:475-80 https://doi.org/10.1007/s11095-007-9359-4 | PubMed

49. **Jiang X,** Patil NA, Azad MAK, Wickremasinghe H, Yu H, Zhao J, et al. (2021) A novel chemical biology and computational approach to expedite the discovery of new-generation polymyxins against life-threatening Acinetobacter baumannii. *Chem Sci* **12**:12211-20 https://doi.org/10.1039/d1sc03460j | PubMed

50. **Roberts KD,** Azad MA, Wang J, Horne AS, Thompson PE, Nation RL, et al. (2015) Antimicrobial activity and toxicity of the major lipopeptide components of polymyxin B and colistin: last-line antibiotics against multidrug-resistant Gram-negative bacteria. *ACS Infect Dis* **1**:568-75 https://doi.org/10.1021/acsinfecdis.5b00085 | PubMed

Peer reviews

Reviewer #1 (Public review):

Summary:

Polymyxins are the last line of drugs to treat gram-negative bacteria-induced multi-drug resistance; however, they cause nephrotoxicity in 60% of patients. In this work, the authors have studied the structure-interaction relationship (SIR) of polymyxins with hPepT2 using computational and experimental methods. Moreover, it is observed that the electrostatic interactions coordinate the hPepT2-Polymyxin interactions; hence, an alanine scanning strategy is used to understand the interactions and derive the polymyxin variants.

Computational methods such as molecular modeling, coarse-grained and all-atom MD simulations, and interaction studies are performed, while the results are validated in the mouse model, which is a great strategy to prove the hypothesis.

Strengths:

A clear understanding of the hPepT2-Polymyxin interactions and the role of electrostatic interactions is one of the very important strengths of the paper. In addition, this work proposes a great pipeline for using computational approaches and experimental validation methods to guide the development of newer antibiotics.

Overall, the study proposes novel polymyxin analogues with reduced or no nephrotoxicity, thereby providing a promising foundation for the rational development of safer lipopeptide antibiotics.

Weaknesses:

This work is very well executed and presented; however, addressing the following concerns might improve the presentation of the work:

(1) The introduction is well articulated; however, including a paragraph on the known inhibitors might be helpful in understanding the current status. In addition, it might also help to introduce Dabs, FADDI variants, Gly-sar and MIPS.

(2) The following details of modeling with AlphaFold2 should be included: how the final structure was selected, what the RMSD and structure alignment of the template are, and the final selected structure. A section on modeling with all the parameter details might be useful for reproducing the structure. In addition, specify how the alanine scanning was performed alongside the structure prediction of polymyxins.

(3) In the all-atom MD simulation method, detailing several parameters might help in reproducing the results: simulation time for each system, water model, system composition, protonation state, box type and dimensions, salt ions and concentration, membrane parameters and ligand parameterization methods. Also, the following details on energy minimization might be useful: minimization algorithm, number of steps for minimization and structure restraints in place.

(4) On page 6, line 210, the MIC is used for the first time; although MIC is given in the abbreviation list, the first occurrence should have a complete name. A one-line explanation of MIC in the introduction or wherever suitable might be better but is not mandatory.

(5) Similarly, Gly-sar is first mentioned on page 8, line 301, but its complete name is only mentioned later on page 10, line 368. This can be addressed if a short description is included in the introduction section.

(6) For coarse-grained MD simulation, why were 2 replicates performed? Most studies perform 3 replicates, which are also good in terms of statistics and error bar calculations. In addition, the authors should specify whether an independent minimization is done for each of the two replicates or whether the minimization step is common for both.

(7) For MD simulation results, giving simulation movies in supplementary results might be a better way to show how the trajectories behaved.

(8) The description of visualisation software such as VMD or PyMol is missing. The authors should specify if any visualization tool is used.

(9) For the mouse model study, the authors claim that FADDI-795 has no observable nephrotoxicity; however, the n=3 shows that a very small number of mouse models were used to make the assumption. In addition, the number of mice used in each experiment is not explicitly mentioned in the methods section.

(10) In Table 2, the column 8 header is not visible.

https://doi.org/10.7554/eLife.111387.1.sa2

Reviewer #2 (Public review):

Summary:

Jiang et al. sought to elucidate the molecular basis of polymyxin antibiotic interaction with the renal transporter hPepT2, a transporter previously implicated in polymyxin-induced nephrotoxicity. They combined molecular dynamics simulations with transporter mutagenesis, functional uptake assays, kinetic analyses, protein expression studies, antibacterial susceptibility testing, and mouse nephrotoxicity experiments to develop a

structure-interaction relationship (SIR) model and apply this model to the rational design of polymyxin analogues.

Overall, the study represents a substantial multidisciplinary effort that integrates computational and experimental approaches. The identification of transporter residues involved in polymyxin recognition and the subsequent design of analogues with reduced hPepT2-mediated uptake provide a valuable framework for developing safer polymyxin antibiotics. In particular, the identification of FADDI-795 as an analogue that retains antibacterial activity while exhibiting reduced nephrotoxicity represents an encouraging proof of concept.

Strengths:

The computational predictions are strengthened by extensive experimental validation, including site-directed mutagenesis, transport kinetics, fluorescence uptake assays, membrane expression analyses, and in vivo toxicity studies. The consistency between multiple independent experimental approaches increases confidence in many of the authors' conclusions.

Weaknesses:

Several conclusions would benefit from a more cautious interpretation. A major limitation is that several transporter mutations substantially altered total or membrane protein expression, making it difficult to distinguish effects on substrate binding from indirect effects caused by impaired transporter stability or trafficking. The authors acknowledge this limitation in the Discussion, but some mechanistic conclusions remain stronger than the available evidence supports.

Similarly, while the proposed binding model is biologically plausible and supported by mutagenesis, it remains an inferred model derived from molecular simulations rather than a direct structural determination. Statements describing the model as "validated" should therefore be moderated to indicate that the experimental data provide support rather than definitive structural confirmation.

The translational implications are promising but remain preliminary. Although FADDI-795 demonstrated reduced nephrotoxicity in the mouse model while maintaining antibacterial activity, no pharmacokinetic studies were presented to demonstrate reduced renal accumulation or altered tissue distribution, and additional efficacy studies in infection models would further strengthen the therapeutic claims.

https://doi.org/10.7554/eLife.111387.1.sa1

Reviewer #3 (Public review):

Summary:

Jiang et al. described findings aimed at interrogating the interactions of the antibiotic polymyxin B with human kidney proteins that mediate nephrotoxicity. Their findings using both computational molecular dynamics simulations and experimental approaches illustrate the importance of aspartic acid residues (D215) in mediating the antibiotic uptake into the cells, and upon mutagenesis with Alanine, the effects are less pronounced. Further, they could modify the antibiotic units interacting with proteins into less toxic peptides with retained antibacterial properties.

Strengths:

I was impressed by this text, which advances the knowledge of how the antibiotic causes human nephrotoxicity and how this could be exploited into less problematic antibiotic peptides.

Weaknesses:

Interactions of Polymyxin B with kidney proteins were not demonstrable in vivo, and with reliable technologies such as X-ray or NMR.

https://doi.org/10.7554/eLife.111387.1.sa0